J Math Imaging Vis (2012) 44:168–184
DOI 10.1007/s10851-011-0319-6

Convex Approximation Technique for Interacting Line Elements Deblurring: a New Approach

Antonio Boccuto · Ivan Gerace · Patrizia Pucci

Published online: 27 September 2011

Abstract The problem of image restoration from blur and noise is studied. A solution of the problem is understood as the minimum of an energy function composed by two terms. The first is the data fidelity term, while the latter is related to the smoothness constraints. The discontinuities of the ideal image are unknown and must be estimated. In particular, the involved images are supposed to be piecewise continuous and with thin and continuous edges. In this paper we assume that the smoothness constraints can be either of the first order, or the second order, or the third order. The energy function that implicitly refers to discontinuities is called dual energy function. To minimize the non-convex dual energy, a GNC (Graduated Non-Convexity) technique is used. The GNC algorithm proposed in this paper is indicated as CATILED, short for Convex Approximation Technique for Interacting Line Elements Deblurring. We also prove in the Appendix the new duality Theorem 3 stated in Sect. 3. Theorem 3 shows that the first convex approximation defined in CATILED has good qualities for the reconstruction. The experimental results, given in Sect. 10, confirm the applicability of the technique.

Keywords Image restoration problem · Regularization · Dual energy functions · Graduated non-convexity

A. Boccuto · I. Gerace · P. Pucci (✉)
Dipartimento di Matematica e Informatica,
Università degli Studi di Perugia, Via Vanvitelli 1, 06123 Perugia, Italy
e-mail: pucci@dmi.unipg.it

A. Boccuto
e-mail: boccuto@dmi.unipg.it

I. Gerace
e-mail: gerace@dmi.unipg.it

1 Introduction

Techniques for restoring digital images have applications in several scientific fields, like biomedicine, astronomy, robotics, and so on. Indeed, in these branches the image is a fundamental tool of investigation. However, sometimes the bad quality of the available images does not allow us to use them immediately. In these cases it is necessary to proceed to a restoration of the involved image, in order to eliminate the presence of noise and the effects of the blur. In this paper the problem of defining suitable models and efficient algorithms for restoring piecewise continuous regular images is investigated. The problem of restoring images deals with estimating the original image, by starting from the observed image and by the characteristic of the blur. In this situation we assume to know the blur mask, while when the mask is unknown the problem is called *blind restoration*. Techniques to solve the blind problem [13, 17, 18] have to refer to the algorithms for the unblind case.

The restoration problem is ill-posed in the sense of Hadamard (cf. [6, 12]), that is, in some cases, the solution neither exists, nor is unique, nor can be stable in presence of noise. Thus, *regularization techniques* (cf. [5, 6, 11, 12, 20, 21]) are useful tools to transform this problem in a well-posed one. The solution is the minimum of a suitable energy function, which is called *primal energy function* and is the sum of two terms. The first measures the data consistency and the latter the faithfulness to the regularity properties of the solution. In particular, concerning the data consistency we use models based on Euclidean norms and the Gaussian regularization.

In order to obtain more realistic restored images, we have to take into account the discontinuities which appear in the intensity field. Edges of the objects arising in the image produce parts of these discontinuities.

Many authors consider just constraints of order one imposing that the solution has to be locally constant. In such a way the restored image looses many characteristics of the original scene. These characteristics could be better recovered imposing smoothness constraints of order two or three for either locally planar or quadric images. In [15] Geman and Reynolds introduced a model with higher order constraints, with solution defined as the minimum of an appropriate energy function. The minimization of this function was performed by a stochastic relaxation algorithm. Moreover they proposed the following strategy to find a more precise solution: starting from the data we first obtain a restoration by the first order model; then we use this image as the starting point for obtaining a restoration by the second order model; finally we use the second order restoration as the starting point for obtaining a reconstruction by the third order model. In [22] Li first uses planar surfaces to model images. Recently, this technique has been successfully adopted also in [19] in the biological comet assay problem. In [19, 22] the smoothness constraints are imposed on the parameters related to the surfaces, in order to obtain local planar results.

In this paper we suppose that the solution satisfies some special constraints, which describe the geometry of the discontinuities. In particular, we assume that adjacent discontinuities cannot be parallel or, alternatively, that lines should be continuous (see Sect. 4).

The energy function which treats implicitly discontinuities is called *dual energy function.* Duality theorems in the literature (cf. [1, 11, 15]) cannot be applied to some prototypes of dual energy functions of interest in applications. For this reason in this paper we present a new duality theorem, see Theorem 3 in Sect. 3.

In general, the dual energy function is not convex and to compute its minimum in [2, 4, 7, 8, 23, 25] the GNC (*Graduated Non-Convexity*) algorithm is used. According to the scheme of this technique, the energy function $\tilde{E}_d$ is approximated by a sequence of functions which converges to $\tilde{E}_d$. Each approximation is minimized by a classical NL-SOR algorithm (that is, *Non-Linear Successive Over Relaxation* algorithm given in [10]), using as starting point the minimum found in the previous approximation. The final result is a good approximation of the global minimum and the choice of the first *convex* approximation of the sequence is crucial. Nikolova in [23] gives a GNC technique to restore blurred images corrupted by noise, while Bedini, Gerace and Tonazzini in [2] use a GNC technique to restore images corrupted only by noise, taking into account the geometry of the discontinuities. In this paper we present a new family of approximating functions to restore images both corrupted by noise and degraded by blur, and we also take into account the constraints of the geometry of discontinuities. This makes the analysis more delicate, but improves the quality of the restored image. The GNC algorithm proposed here is called CATILED (*Convex Approximation Technique for Interacting Line Elements Deblurring*). Moreover, from Theorem 3 it is easily seen that even the first convex approximation of the dual energy function is almost "optimal" in order to reconstruct the original image, since it preserves the discontinuities.

The quality of the reconstruction is also apparent from a quantitative point of view, given by the *mean squared errors*—MSE—between the reconstructed image and the ideal image, cf. Tables 1–3 of Sect. 10.

In Sect. 2 the problem of the image restoration is presented. In Sect. 3 we define the dual energy and prove the duality theorem. In Sect. 4 we deal with the interactions between line variables. In Sect. 5 the relations between primal and dual energy functions are investigated under suitable constraints on the geometry of the discontinuities. In Sect. 6 the GNC technique is explained, while in Sect. 7 the CATILED algorithm is defined. In Sect. 8 we present the descent algorithm used in the new GNC technique. In Sect. 9 we find the primal energy function of the first convex approximation in CATILED. In Sect. 10 some experimental results are presented, which illustrate how the CATILED algorithm works in the reconstruction of noise and noiseless images. Concluding remarks are given in Sect. 11, while in the Appendix the proof of the main Theorem 3 is displayed.

2 The Problem of Image Restoration

The problem of image restoration consists in reconstructing the original image from an image blurred and/or corrupted by noise. In the sequel we assume that all intensities of our involved pixels are put into one column, with the rule that $(i, j) < (i', j')$ if and only if $i < i'$ or $i = i'$ and $j < j'$. The direct problem can be formulated as follows:

$$\boldsymbol{y} = A\boldsymbol{x} + \boldsymbol{n},$$

where the vectors $\boldsymbol{x}$, $\boldsymbol{y}$, of dimension n^2, are respectively the original image and the observed one. In particular, the elements of these vectors indicate the luminosity intensity of pixels in the corresponding image. The vector $\boldsymbol{n}$, of dimension n^2, is the additive noise on the image, which we assume to be independent and identically distributed (i.i.d.) Gaussian, with zero mean and known variance. The $n^2 \times n^2$ matrix A is a linear operator, which represents the translation invariant blur acting on the image. To obtain a blurred image, each pixel of original image is set to a weighted average of its neighbors. Given a positive matrix $M \in \mathbb{R}^{(2h+1)\times(2h+1)}$, called *blur mask,* the entries of the

matrix A can be defined by:

$$a_{(i,j),(i+w,j+v)} = \begin{cases} \frac{m_{h+1+w,h+1+v}}{\nu_{i,j}}, & \text{if } |w|, |v| \le h, \\ 0, & \text{otherwise,} \end{cases}$$

where $\nu_{i,j} = \sum_{i=\kappa}^{\eta} \sum_{j=\ell}^{\delta} m_{i,j}$, $\kappa = \max\{1, i-2h+1\}$, $\eta = \min\{n, i+2h+1\}$, $\ell = \max\{1, j-2h+1\}$ and $\delta = \min\{n, j+2h+1\}$. Here, in lexicographic notation, the generic index $((i,j),(h,l))$ of matrix A is supposed to be equal to $((j-1)n+i,(l-1)n+h)$.

The image restoration problem is the problem of finding an estimation $\boldsymbol{x}$ of the unknown original image given the blurred image $\boldsymbol{y}$, the matrix A and the variance of the noise σ^2. This is an ill-posed inverse problem in the Hadamard sense.

Let a *clique* c of order k be the subset of points of a square gride on which the k-th order finite difference is defined. We indicate with the symbol C_k the set of all cliques of order k.

More precisely, we consider, for $k=1$,

$$C_1 = \{c = \{(i,j),(h,l)\} : i = h,\ j = l+1 \text{ or } i = h+1,\ j = l\},$$

for $k=2$,

$$C_2 = \{c = \{(i,j),(h,l),(r,q)\} : i = h = r,\ j = l+1 = q+2, \text{ or } i = h+1 = r+2,\ j = l = q\},$$

and $k=3$,

$$C_3 = \{c = \{(i,j),(h,l),(r,q),(w,z)\} : i = h = r = w,\ j = l+1 = q+2 = z+3, \text{ or } i = h+1 = r+2 = w+3,\ j = l = q = z\}.$$

We denote the k-th order finite difference operator of the vector $\boldsymbol{x}$ associated with the clique c by $D_c^k\boldsymbol{x}$. Namely, if $c = \{(i,j),(h,l)\} \in C_1$, then

$$D_c^1\boldsymbol{x} = x_{i,j} - x_{h,l},$$

if $c = \{(i,j),(h,l),(r,q)\} \in C_2$, then

$$D_c^2\boldsymbol{x} = x_{i,j} - 2x_{h,l} + x_{r,q},$$

and if $c = \{(i,j),(h,l),(r,q),(w,z\} \in C_3$, then

$$D_c^3\boldsymbol{x} = x_{i,j} - 3x_{h,l} + 3x_{r,q} - x_{w,q}.$$

Let us now introduce the auxiliary variables associated with the discontinuities of the image $\boldsymbol{x}$. A good estimate of the discontinuities improves the quality of restored image (cf. [5, 8, 14]). Such variables have the role of eliminating the regularity constraint, where discontinuities should appear.

To every clique c we associate a non-negative weight b_c, called *line variable*; in particular, the zero value corresponds to a discontinuity in the involved image in c. The vector $\boldsymbol{b}$ is the set of all line variables b_c. Thus, the original image is considered as a pair $(\boldsymbol{x},\boldsymbol{b})$, where $\boldsymbol{x}$ is the vector of the grey intensity of pixels and $\boldsymbol{b}$ is the vector of the set of all components b_c, $c \in C_k$, with fixed $k \in \{1,2,3\}$; $\boldsymbol{x}$ and $\boldsymbol{b}$ are called *intensity process* and *line process* respectively.

A regularized solution of restoration problem is obtained as the minimum of the following function, called *primal energy function*:

$$E(\boldsymbol{x},\boldsymbol{b}) = \|\boldsymbol{y} - A\boldsymbol{x}\|^2 + \sum_{c\in C_k} \left[\lambda^2 (D_c^k\boldsymbol{x})^2 b_c + \beta(b_c)\right], \tag{1}$$

where the first term measures faithfulness of the solution to data and the second one is a regularization term, which imposes a smoothness condition on $\boldsymbol{x}$. The parameter λ^2 reflects the confidence that we have in the data. In particular, if λ^2 tends to zero, we get the perfect confidence in the data; while, if λ^2 tends to ∞, the perfect confidence in the a priori information is obtained. The function β is assumed to be strictly decreasing on its domain B, to avoid having too many discontinuities in the restored image.

Throughout this paper, we often refer to the following case (cf. also [2, 5, 7, 8, 14]):

$$B = \{0,1\}, \qquad \beta(b) = \alpha(1-b), \tag{2}$$

where α is a suitable positive parameter.

3 Dual Energy Function

To find the minimum of the primal energy function (1), first we minimize with respect to the line process $\boldsymbol{b}$. The dual energy function $E_d(\boldsymbol{x})$ can be defined as (cf. [8, 11, 15]):

$$E_d(\boldsymbol{x}) = \inf_{\boldsymbol{b}\in B^{|C_k|}} E(\boldsymbol{x},\boldsymbol{b}),$$

where the symbol $|C_k|$ denotes the cardinality of the set C_k. Namely E_d is of the form:

$$E_d(\boldsymbol{x}) = \|\boldsymbol{y} - A\boldsymbol{x}\|^2 + \sum_{c\in C_k} g(D_c^k\boldsymbol{x}), \tag{3}$$

where

$$g(t) = \inf_{b\in B}\{\lambda^2 b t^2 + \beta(b)\},$$

called *interaction function*, associates a cost to every value of the gradient of the image and does not depend on the clique.

For example, consider the expression of the dual energy function given in (3) when β is defined by (2); in this case, the interaction function has the following form:

$$g(t) = \min_{b\in\{0,1\}} \{\lambda^2 b t^2 + \alpha(1-b)\},$$

that is

$$g(t) = \min\{\lambda^2 t^2, \alpha\} = \begin{cases} \lambda^2 t^2, & \text{if } |t| < \frac{\sqrt{\alpha}}{\lambda}, \\ \alpha, & \text{otherwise.} \end{cases} \tag{4}$$

The quantity $s = \sqrt{\alpha}/\lambda$ has the meaning of a *threshold* for creating a discontinuity (see [8, 24]).

Geman and Reynolds [15] and Charbonnier et al. [11] established two different versions of the duality theorem. These sufficient criteria give a correspondence between the primal and dual energy functions, and we report them here for the convenience of the reader.

Theorem 1 (Geman and Reynolds, [15]) *Fix $\lambda \in \mathbb{R}$, $\lambda \neq 0$. Let $g : \mathbb{R} \to \mathbb{R}$ be a function, satisfying the following properties*:

(1) $g(0) = 0$,
(2) $f(t) = g(\sqrt{t})$ *is concave*,
(3) $\lim_{t\to\infty} g(t) = \alpha$, *with* $\alpha > 0$.

Then there exists a function β, defined in a suitable interval $[0, b_M]$, such that:

$$g(t) = \inf_{0\le b\le b_M} \{\lambda^2 b t^2 + \beta(b)\},$$

and:

(4) $\beta(0) = \alpha$,
(5) β *is strictly decreasing*,
(6) $\beta(b_M) = 0$.

Note that assumption (3) of Theorem 1 is not always satisfied in examples of interest in applications. In particular, the well-known Huber function g^* defined in Sect. 7 does not verify (3). Moreover, Geman and Reynolds did not give any regularity condition on the functions g and β. The function $g(t) = \min\{\lambda^2 |t|, \alpha\}$, where $\alpha > 0$ and $\lambda > 0$ are fixed parameters, satisfies all the assumptions of Theorem 1, but an easy calculation shows that

$$\beta(b) = \begin{cases} \alpha - b\frac{\alpha^2}{\lambda^2}, & \text{if } b \in [0, \lambda^2/2\alpha), \\ \frac{\lambda^2}{4b}, & \text{if } b \in [\lambda^2/2\alpha, \infty), \\ 0, & \text{if } b = \infty. \end{cases}$$

Namely, using the notation of Theorem 1, we have $b_M = \infty$.

Theorem 2 (Charbonnier, Blanc–Féraud, Aubert and Barlaud, [11]) *Fix $\lambda \in \mathbb{R}$, $\lambda \neq 0$. Let $g : \mathbb{R} \to \mathbb{R}$ be an even function, satisfying the following conditions*:

(i) $g(t) \ge 0, \quad \forall t; \quad g(0) = 0$,
(ii) g *is of class* $C^1(\mathbb{R})$,
(iii) $g' \ge 0 \quad \text{in } \mathbb{R}_0^+$,
(iv) $\frac{g'(t)}{2t}$ *is continuous and strictly decreasing in* $\mathbb{R}^+$,
(v) $\lim_{t\to\infty} \frac{g'(t)}{2t} = 0$,
(vi) $\lim_{t\to 0^+} \frac{g'(t)}{2t} = b_M$, *with* $0 < b_M < \infty$.

Then there exists a strictly convex decreasing function $\beta : (0, b_M] \to [0, \alpha)$, where

$$\alpha = \lim_{t\to\infty} \left[g(t) - \frac{1}{2} t\, g'(t) \right],$$

such that

$$g(t) = \inf_{0<b\le b_M} \{\lambda^2 b t^2 + \beta(b)\}.$$

The function g, given in (4) see also Fig. 1, does not satisfy the assumptions of Theorem 2. Hence, an alternative version of the duality theorem is required in our context. Furthermore, the duality result given in the next theorem is a sufficient and necessary criterion.

Theorem 3 *Fixed $\lambda \in \mathbb{R}$ with $\lambda \neq 0$, assume that*:

(a) $B = \bigcup_{j=1}^m I_j$ *is a subset of* $\mathbb{R}_0^+$, *consisting of the union of bounded intervals or singletons, such that* $\overline{I_h} \cap \overline{I_j} = \emptyset$ *for all* $h \neq j$;
(b) $\beta : B \to \mathbb{R}$ *is a continuous function, bounded from below, strictly decreasing in B and strictly convex on each interval* I_j.

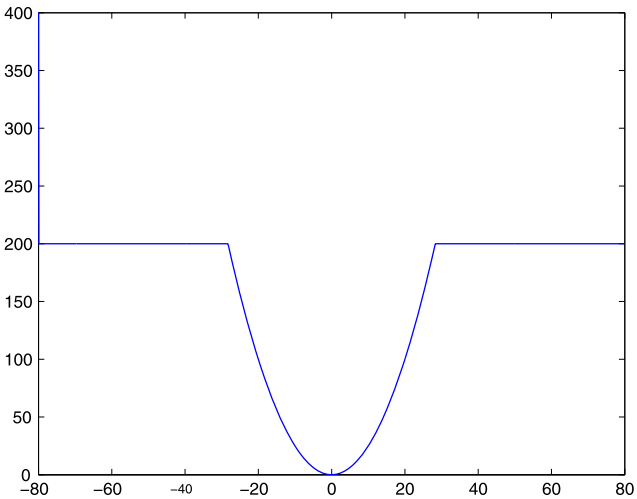

Fig. 1 The function g in (4) with $\alpha = 10$ and $\lambda = 1$

Put

$$g(t) = \inf_{b\in B}\{\lambda^2 bt^2 + \beta(b)\}, \quad t \in \mathbb{R}. \tag{5}$$

Then

(c) *g is even, non-decreasing on $\mathbb{R}_0^+$ and of class $\mathrm{Lip}_{\mathrm{loc}}(\mathbb{R})$;*
(d) *the function $f(t) = g(\sqrt{t})$, $t \geq 0$, is continuous, non-decreasing, concave in $\mathbb{R}_0^+$, not differentiable at most in a finite set of points of $\mathbb{R}^+$. The derivative f' on its domain is a continuous and non-increasing function.*

Moreover

$$f(0) = \lim_{b\to \sup B} \beta(b). \tag{6}$$

Conversely, if $g : \mathbb{R} \to \mathbb{R}$ and $f : \mathbb{R}_0^+ \to \mathbb{R}$ are two functions, satisfying (c), (d) respectively, then there exist a set $B \subset \mathbb{R}_0^+$ and a function β, satisfying (a), (b), (5) and (6).

The proof of Theorem 3 is presented in the Appendix of the paper.

4 Interaction Between Line Variables

To consider the possible geometry features between close line variables, in the expression of the energy function (1) we add a term $Q(\boldsymbol{b})$, that represents our a priori knowledge about the structure of discontinuities. Thus (1) becomes

$$E(\boldsymbol{x}, \boldsymbol{b}) = \|\boldsymbol{y} - A\boldsymbol{x}\|^2 + \sum_{c\in C_k} \left[\lambda^2 (D_c^k \boldsymbol{x})^2 b_c + \beta(b_c)\right] + Q(\boldsymbol{b}). \tag{7}$$

In particular, two possible cases occur: when $Q(\boldsymbol{b})$ consists in a constraint which guarantees the continuation of the line elements in the restored image and when $Q(\boldsymbol{b})$ avoids adjacent parallel line elements, which arise from the blur. The first case is very important, since the discontinuities of an image are often closed curves, that is no gaps occur; the latter is also relevant, since the restored blurred image should not present parallel lines, which arise from the blur and not from the ideal image. At the moment we are not able to overcome both problems at once, so that, according to a possible a priori acknowledgement, we choice the constraint to adopt taking a special form of $Q(\boldsymbol{b})$.

For instance, if we impose the continuation of the line elements in the restored image, in order to define an appropriate $Q(\boldsymbol{b})$ we take the total orders $\preceq^1$, $\preceq^2$ and $\preceq^3$ on C_1, C_2 and C_3 defined by

$$\{(i,j),(i-1,j)\} \preceq^1 \{(i,h),(i-1,h)\} \quad \Leftrightarrow \quad j \leq h,$$

$$\{(i,j),(i,j-1)\} \preceq^1 \{(h,j),(h,j-1)\} \quad \Leftrightarrow \quad i \leq h,$$

$$\{(i,j),(i-1,j),(i-2,j)\} \preceq^2 \{(i,h),(i-1,h),(i-2,h)\} \quad \Leftrightarrow \quad j \leq h,$$

$$\{(i,j),(i,j-1),(i,j-2)\} \preceq^2 \{(h,j),(h,j-1),(h,j-2)\} \quad \Leftrightarrow \quad i \leq h,$$

$$\{(i,j),(i-1,j),(i-2,j),(i-3,j)\} \preceq^3 \{(i,h),(i-1,h),(i-2,h),(i-3,h)\} \quad \Leftrightarrow \quad j \leq h,$$

$$\{(i,j),(i,j-1),(i,j-2),(i,j-3)\} \preceq^3 \{(h,j),(h,j-1),(h,j-2),(h,j-3)\} \quad \Leftrightarrow \quad i \leq h.$$

By $c-1$ we denote the maximal clique that precedes $c \in C_k$ in the order $\preceq^k$, that is

$$c - 1 = \sup\{\tilde{c} \in C_k : \tilde{c} \preceq^k c\}.$$

We use the convention that if $c-1$ does not exist then $b_{c-1} = 0$. In this case a possible expression for Q is given by

$$Q(\boldsymbol{b}) = \sum_{c\in C_k} \rho(b_c, b_{c-1}), \tag{8}$$

where $\rho = \rho(u,v)$ is a regular function on its natural domain $\Omega \supset B^2$, non-increasing in both u and v, and such that $\partial^2_{u,v}\rho(\tilde{u},\tilde{v}) \neq 0$ at some point $(\tilde{u},\tilde{v})$.

A good choice of ρ, when β in (7) is as in (2), is given for $(u,v) \in B^2 = \{0,1\}\times\{0,1\}$

$$\rho(u,v) = \varepsilon(1-u)(1-v), \tag{9}$$

where $\varepsilon \in (-\alpha, 0)$, and $\alpha > 0$ is the constant in (2).

Similarly, we proceed to avoid adjacent parallel lines. For this aim we introduce the total orders $\preceq_1$, $\preceq_2$ and $\preceq_3$, defined on C_1, C_2 and C_3, respectively, by

$$\{(i,j),(i-1,j)\} \preceq_1 \{(h,j),(h-1,j)\} \quad \Leftrightarrow \quad i \leq h,$$

$$\{(i,j),(i,j-1)\} \preceq_1 \{(i,h),(i,h-1)\} \quad \Leftrightarrow \quad j \leq h,$$

$$\{(i,j),(i-1,j),(i-2,j)\} \preceq_2 \{(h,j),(h-1,j),(h-2,j)\}$$

$$\Leftrightarrow \quad i \le h,$$

$$\{(i,j),(i,j-1),(i,j-2)\} \preceq_2 \{(i,h),(i,h-1),(i,h-2)\}$$

$$\Leftrightarrow \quad j \le h,$$

$$\{(i,j),(i-1,j),(i-2,j),(i-3,j)\}$$

$$\preceq_3 \{(h,j),(h-1,j),(h-2,j),(h-3,j)\}$$

$$\Leftrightarrow \quad i \le h,$$

$$\{(i,j),(i,j-1),(i,j-2),(i,j-3)\}$$

$$\preceq_3 \{(i,h),(i,h-1),(i,h-2),(i,h-3)\}$$

$$\Leftrightarrow \quad j \le h.$$

Again $c-1$ is the maximal clique that precedes $c \in C_k$ but now in the order $\preceq_k$, so that $c-k$ is the maximal clique that precedes $c-(k-1)$ in the sense of $\preceq_k$. Again if $c-k$ does not exist then $b_{c-k}=0$. A useful form of Q is here given by

$$Q(\boldsymbol{b}) = \sum_{c \in C_k} \rho(b_c, b_{c-k}), \tag{10}$$

where $\rho = \rho(u,v)$ is a regular function on its natural domain $\Omega \supset B^2$, non-decreasing in both u and v, and such that $\partial^2_{u,v}\rho(\tilde{u},\tilde{v}) \neq 0$ at some point $(\tilde{u},\tilde{v})$. For instance, when β in (7) is as in (2), then ϱ can be defined in B^2 as in (9), with now $\varepsilon > 0$.

Note that in a second order reconstruction we inhibit of closed triple parallel discontinuities. Indeed, differently from the first order reconstruction, in this case double parallel edges have not to be inhibit. In fact, in many cases, a double second order edge corresponds just to a simple first order discontinuity. similarly in a third order reconstruction we inhibit the presence of four adjacent parallel discontinuities.

5 Correspondence Between Primal and Dual Energy Functions with $Q \not\equiv 0$

Let us consider the energy function given as in (7). In particular, let Q be as either in (8) or in (10). In both cases, it is difficult to compute explicitly the dual energy function, and so we consider an approximation $\xi_{c-j}(\boldsymbol{x})$ of the variable b_{c-j}, defined as

$$\begin{aligned}\xi_{c-j}(\boldsymbol{x}) &= \arg_{c-j} \min_{\boldsymbol{b} \in B^{|C_k|}} E(\boldsymbol{x},\boldsymbol{b}) \\ &= \arg \min_{b \in B} \{\lambda^2 (D^k_{c-j}(\boldsymbol{x}))^2 b + \beta(b)\},\end{aligned}$$

where E is as in (1), and either $c-j = c-1$ if Q is as in (8), or $c-j = c-k$ if Q is as in (10). Of course, ξ_{c-j} depends only on $D^k_{c-j}(\boldsymbol{x})$, so, without loss of generality, we can write $\xi_{c-j}(\boldsymbol{x}) = \mu(D^k_{c-j}(\boldsymbol{x}))$. Hence we approximate the primal energy in (7) as follows

$$\begin{aligned}\tilde{E}(\boldsymbol{x},\boldsymbol{b}) =& \|\boldsymbol{y} - A\boldsymbol{x}\|^2 + \sum_{c \in C_k} \big[\lambda^2 (D^k_c \boldsymbol{x})^2 b_c + \beta(b_c) \\ &+ \rho(b_c, \mu(D^k_{c-j}(\boldsymbol{x})))\big],\end{aligned}$$

with the convention that, if $c-j$ does not exist, then $\rho(b_c, \mu(D^k_{c-j}(\boldsymbol{x}))) = 0$. Note that now $\tilde{E}_d$ deals only with non-interacting line elements. The corresponding dual energy is

$$\begin{aligned}\tilde{E}_d(\boldsymbol{x}) =& \|\boldsymbol{y} - A\boldsymbol{x}\|^2 \\ &+ \sum_{c \in C_k} \psi(D^k_c(\boldsymbol{x}), D^k_{c-j}(\boldsymbol{x})),\end{aligned} \tag{11}$$

where

$$\psi(u,v) = \inf_{b \in B} \{\lambda^2 b u^2 + \beta(b) + \rho(b, \mu(v))\}.$$

In the particular case in which B, β are as in (2), and ρ is as in (9), with either $\varepsilon \in (-\alpha, 0)$ if Q is as in (8), or $\varepsilon > 0$ if Q is as in (10), we have that

$$\mu(v) = \begin{cases} 1, & \text{if } |v| < s = \frac{\sqrt{\alpha}}{\lambda}, \\ 0, & \text{otherwise.} \end{cases}$$

Hence we get

$$\psi(u,v) = \begin{cases} g(u) = \overline{g}(u,0), & \text{if } |v| < s, \\ g_\varepsilon(u) = \overline{g}(u,\varepsilon), & \text{if } |v| \ge s, \end{cases} \tag{12}$$

where $\overline{g} : \mathbb{R} \times (-\alpha, \infty) \to \mathbb{R}^+_0$ is defined by

$$\overline{g}(u,v) = \begin{cases} \lambda^2 u^2, & \text{if } |u| < \sqrt{\alpha + v}/\lambda, \\ \alpha + v, & \text{if } |u| \ge \sqrt{\alpha + v}/\lambda. \end{cases}$$

The function ψ is given in Fig. 2(c).

6 GNC Algorithms

In this section we present an algorithm to minimize the dual energy $\tilde{E}_d$. In general, $\tilde{E}_d$ is not convex. The solution of the algorithms for minimizing a non-convex function depends on the choice of the starting point. To give an adequate choice of the initial point, a standard technique is to find a finite family of approximating functions $\{\tilde{E}^{(p)}_d\}_p$, such that the first one is convex and the last one is the original dual energy function (cf. [2, 4, 7, 8, 23, 25]), and then to apply the following algorithm:

`initialize` x;
`while` $\tilde{E}_d^{(p)} \neq \tilde{E}_d$ `do`

- `find the minimum of the function` $\tilde{E}_d^{(p)}$ `starting from the initial point` x;
- $x = \arg\min \tilde{E}_d^{(p)}$;
- `update the parameter` p.

The algorithm above is called GNC (*Graduated Non-Convexity*) algorithm. The first GNC algorithm was proposed by Blake and Zisserman [7, 8], who approximate the dual energy in (3) where the function g is defined in (4), with $A = I$, the identity matrix. Bedini, Gerace and Tonazzini [2] proposed an extension of GNC algorithm, called E-GNC (*Extended Graduated Non-Convexity*), for the dual energy given in (11), ψ in (12) and $A = I$, which takes alternatively into account the constraint of non-parallelism or the line continuation constraint, in accord with the choice of $Q(\boldsymbol{b})$ either in (8) or in (10). Moreover, Nikolova [23] studied the dual energy in (3), where g is given as in (4), but A is an arbitrary blur matrix, not necessarily equal to the identity matrix.

7 The CATILED Algorithm

Here, we focus our attention on finding a family of approximating functions of the dual energy function (11). In this function we choose ψ as in (12), in such a way that, differently from Nikolova [23], it is possible to consider geometry of discontinuities. Moreover, differently from Blake and Zissermann [7, 8] and Bedini, Gerace and Tonazzini [2], A is taken to be as an arbitrary matrix.

Thus we deal with the problem of deblurring, which takes into account the constraints of the geometry of discontinuities. The Hessian matrix associated with faithfulness to the data in (11), namely to the first term $\|\boldsymbol{y} - A\boldsymbol{x}\|^2$, is

$$\Theta = 2\,A^T A, \tag{13}$$

which is positive semidefinite.

Now we deal with the problem of finding a convex approximation of the regularization term in (11). Let us first find a $C^1(\mathbb{R}^2)$-approximation of the function ψ in (12): the discontinuity points of the derivative of the function $g(u)$ in (12) are located in $u = \pm s$. Thus, we interpolate in this function two quadratic arcs in such a way to eliminate these discontinuities. In the same way it is possible to construct a $C^1(\mathbb{R}^2)$-approximation of the function $g_\varepsilon(u)$ in (12). To eliminate the discontinuities in the function ψ in (12) and in its derivatives in $v = \pm s$, we interpolate two quadratic arcs between $g(u)$ and $g_\varepsilon(u)$ in $v = s$, and two other arcs in $v = -s$. Namely, for $p \in (0, 1]$,

$$\psi^{(p)}(u, v) = \begin{cases} \overline{g}^{(p)}(u, 0), & \text{if } |\,v\,| \leq s, \\ a^{(p)}(u)(|\,v\,| - s)^2 + \overline{g}^{(p)}(u, 0), & \\ \quad \text{if } s < |\,v\,| \leq \frac{\varphi(p)+s}{2}, & \\ -a^{(p)}(u)[\,|\,v\,| - \varphi(p)]^2 + \overline{g}^{(p)}(u, \varepsilon), & \\ \quad \text{if } \frac{\varphi(p)+s}{2} < |\,v\,| < \varphi(p), & \\ \overline{g}^{(p)}(u, \varepsilon), & \text{otherwise,} \end{cases} \tag{14}$$

where $\varphi(p) = s + pz$, with $z > 0$ arbitrary, and $s = \sqrt{\alpha}/\lambda$. The function $\overline{g}^{(p)}(u, v)$ is

$$\overline{g}^{(p)}(u, v) = \begin{cases} \lambda^2 u^2 & \text{if } |u| < q_p(v), \\ \alpha - \frac{\tau^{(p)}}{2}\big[|u| - r_p(v)\big]^2 & \text{if } q_p(v) \leq |u| \leq r_p(v), \\ \alpha & \text{if } |u| > r_p(v), \end{cases}$$

where

$$q_p(v) = \frac{\sqrt{\alpha + v}}{\lambda^2}\left(\frac{2}{\tau^{(p)}} + \frac{1}{\lambda^2}\right)^{-1/2}, \tag{15}$$

with $\tau^{(p)} = \tau^*/p$, where τ^* is an arbitrary positive real constant, and

$$r_p(v) = \frac{\alpha + v}{\lambda^2\, q_p(v)}. \tag{16}$$

The function $a^{(p)}(u)$ is given by:

$$a^{(p)}(u) = 2\,\frac{\overline{g}^{(p)}(u, \varepsilon) - \overline{g}^{(p)}(u, 0)}{[\varphi(p) - s]^2}.$$

Any approximation $\psi^{(p)}$ with $p \in (0, 1]$ is a $C^1(\mathbb{R}^2)$-approximation of ψ in (12).

Let ψ^* be a first convex approximation of ψ of class $C^1(\mathbb{R}^2)$. In this paper, we take

$$\psi^*(u, v) = g^*(u) \tag{17}$$

for all $(u, v) \in \mathbb{R}^2$, where

$$g^*(u) = \begin{cases} \lambda^2 u^2, & \text{if } |\,u\,| < q_1(0), \\ 2\,\lambda^2 q_1(0)\,|u| - \lambda^2 q_1^2(0), & \text{if } |\,u\,| \geq q_1(0) \end{cases}$$

for all $u \in \mathbb{R}$. This function $g^*(u)$ is well known as the Huber function [9].

For $p = 0$ we put $\psi^{(0)} \equiv \psi$. For $p \in [1, 2]$, the approximating functions are defined as follows:

$$\psi^{(p)} = (p - 1)\,\psi^* + (2 - p)\psi^{(1)}, \tag{18}$$

where ψ^* and $\psi^{(1)}$ are given in (17) and (14) respectively. In our GNC algorithm the parameter p varies linearly from 2 to 0. In Figs. 2(a), 2(b) and 2(c), the graphs of the functions $\psi^{(2)} \equiv \psi^*$, $\psi^{(1)}$ and $\psi^{(0)} \equiv \psi$ are given respectively. We note that, thanks to the presence of z and τ^*, the approximating functions $\psi^{(p)}$ are of class $C^1(\mathbb{R}^2)$ for each $p \in (0, 2]$, as required in the numerical algorithm. The GNC algorithm proposed in this paper is indicated as CATILED, short for *Convex Approximation Technique for Interacting Line Elements Deblurring*.

When $\varepsilon = 0$, the family of approximations (14) and (18) reduces exactly to the one considered in [23] by Nikolova in the case of non-strictly convex data fidelity term and truncated quadratic stabilizer.

8 Descent Algorithms

To minimize the different approximations, the NL-SOR (*Non-Linear Successive Over Relaxation*) algorithm [10] is used. In this algorithm, the mth iteration is defined for all $i, j = 1, \ldots, n$ by

$$x_{i,j}{}^{(m+1)} = x_{i,j}{}^{(m)} - \omega \frac{\partial_{x_{i,j}} \tilde{E}_d^{(p)}(\boldsymbol{x})}{T_{i,j}},$$

where $0 < \omega < 2$ is the *NL-SOR parameter*, that influences the speed of convergence, and $T_{i,j}$ is an upper bound on the second derivative, i.e:

$$T_{i,j} \geq \partial^2_{x_{i,j}} \tilde{E}_d^{(p)}(\boldsymbol{x}), \quad i, j = 1, \ldots, n.$$

The same algorithm was later used by Blake and Zisserman [8] and Bedini, Gerace and Tonazzini [2]. The convergence of the first convex approximation, that is when $p = 2$, has been proved by Brewster and Kannan in [10] in an interval smaller than $(0, 2)$ for ω. We have experimentally noted that the speed of convergence of the successive approximations depends of the quality of the minimum found in the first approximation. Thus, to have an efficient GNC algorithm, both in the sense of computational costs and in the quality of restoration, it is necessary to choose a suitable first convex approximation. In the next section we show that this approximation works for our purposes, since it satisfies the duality Theorem 3. In passing we also recall that in [25] an interior point method is adopted in a GNC algorithm in order to minimize a functional possibly not convex.

9 Primal Energy Function of the First Convex Approximation

Let g^* be the first convex approximation function given in (17) and $f^*(t) = g^*(\sqrt{t})$ for all $t \geq 0$. Hence, by a direct

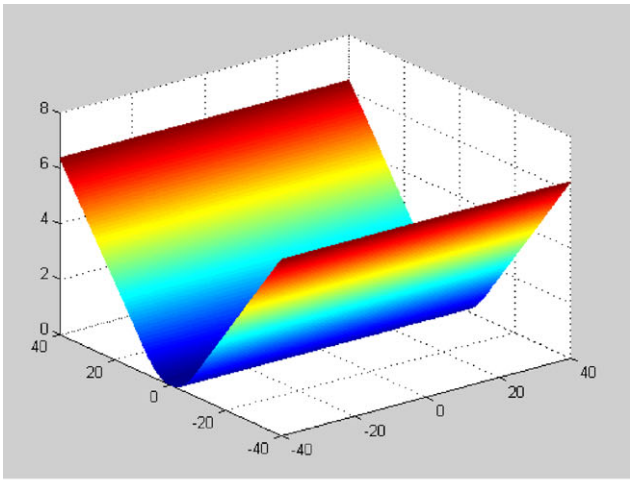

(a)

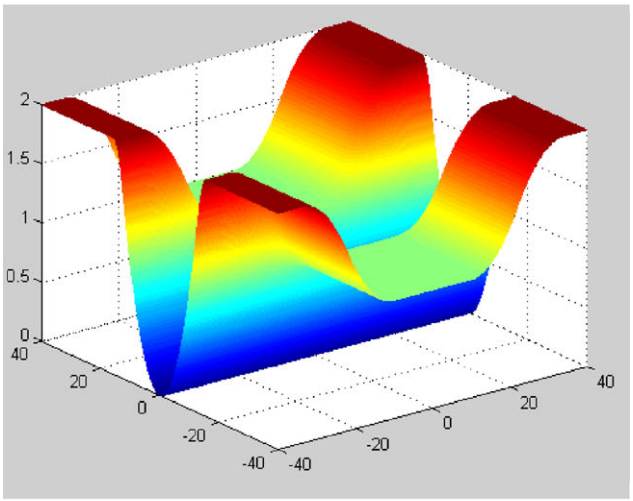

(b)

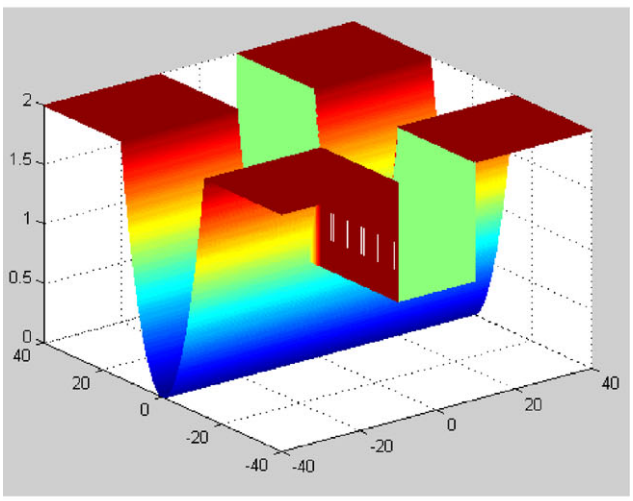

(c)

Fig. 2 (**a**) Function $\psi^{(2)} \equiv \psi^*$; (**b**) function $\psi^{(1)}$; (**c**) function $\psi^{(0)} \equiv \psi$. They are obtained with $\alpha = 1$, $\lambda = 0.1$ and $\varepsilon = 1$

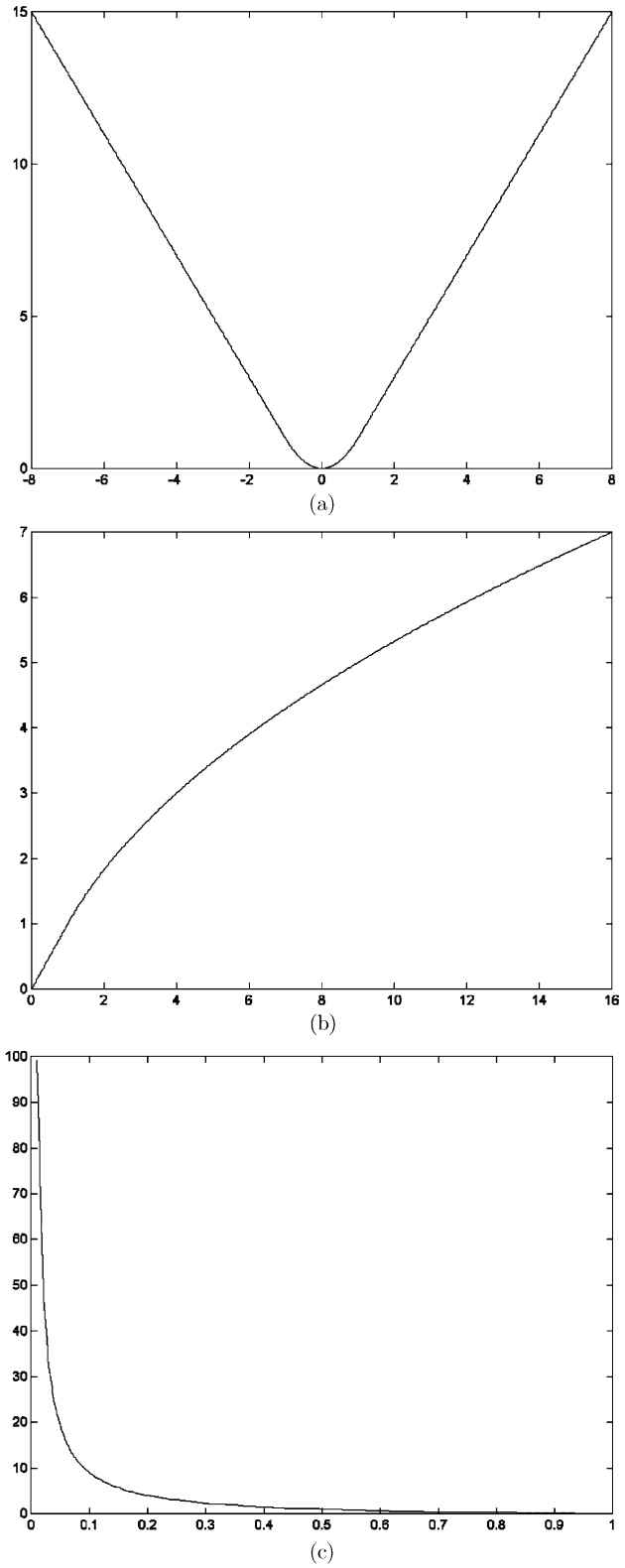

Fig. 3 (**a**) Function g^*; (**b**) function f^*; (**c**) function β^*. They are obtained with $\lambda = 1$ and $q = 1$

calculation, f^* and g^* satisfy the conditions (c) and (d) of Theorem 3, so that they are adequate to deal with implicit discontinuities. We can construct the set B^* and the function β^* satisfying (a), (b) and (5) of Theorem 3. Indeed, following the proof of this theorem, we put $B^* = \{\zeta/\lambda^2 : \zeta \in \Xi\}$, where Ξ is the set of the values attained by $f^{*\prime}$, namely $B^* = (0, 1]$. The function $\beta^*(b)$, $b \in B^*$, is the y-coordinate of the intersection point between the y-axis and any tangent line to the graph of f^* whose angular coefficient is $\lambda^2 b$. The function β^* is well-defined by

$$\beta^*(b) = \lambda^2 q_1^2(0)\left(\frac{1}{b} - 1\right) \quad \forall b \in B^*.$$

In Figs. 3(a), 3(b) and 3(c), there are the graphs of the functions g^*, f^*, β^* respectively. However, the first approximation g^* does not take into account of the interaction between discontinuities.

10 Experimental Results

In this section we first show, by some experimental results, how the CATILED algorithm can inhibit the formation of double lines or can favor the line continuation. Then we present concrete examples which illustrate how the use of higher order differential operators $D_c^k \boldsymbol{x}$, $k = 2, 3$, improves the quality of the reconstructed image $\boldsymbol{x}$.

To evaluate properly the quality of the reconstructed images, we initially start from an ideal image, that is, we first blur it and then, using CATILED algorithm, we try to reconstruct the original image. Even if this could seem artificial, on the other hand this allow us to evaluate the error in the reconstruction. In any case, to avoid any misunderstanding, we present the reconstruction also of an image not blurred artificially.

In the first set of examples below the choice of the involved free parameters α, λ and ε is taken to show the different quality of the reconstructed images and how relevant is the fact that ε can be taken different from 0. In the second set of examples below the parameters α and λ are chosen by an algorithm proposed in [16], while the parameter ε is either α or $-\alpha$ depending of the involved constraint. We recall in passing that there are several algorithms available in literature for this aim, see e.g. [3, 20, 21, 26].

Let us first examine the adjacent parallel lines inhibition constraint. In Fig. 4(a) the first considered image of dimension 128×128 (*Synthetic1*) appears. In Fig. 4(b) there is the image Synthetic1 blurred by the following blur mask:

$$M_1 = \begin{pmatrix} 1 & 1 & 1 & 1 & 1 \\ 1 & 1 & 1 & 1 & 1 \\ 1 & 1 & 1 & 1 & 1 \\ 1 & 1 & 1 & 1 & 1 \\ 1 & 1 & 1 & 1 & 1 \end{pmatrix}. \tag{19}$$

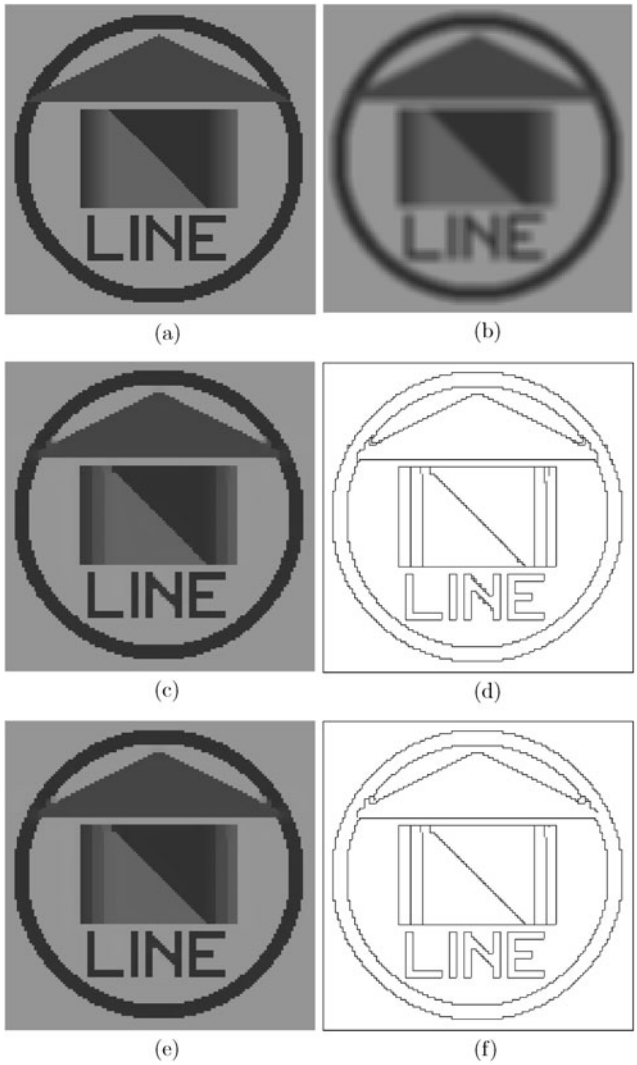

Fig. 4 (**a**) Image Synthetic1; (**b**) image Synthetic1 blurred by mask (19); (**c**) restoration obtained by Nikolova's algorithm ($\lambda = 0.5$ and $\alpha = 10$) and (**d**) its line elements; (**e**) restoration obtained by the CATILED algorithm with the non-parallelism constraint ($\lambda = 0.5$, $\alpha = 10$ and $\varepsilon = 150$) and (**f**) its line elements

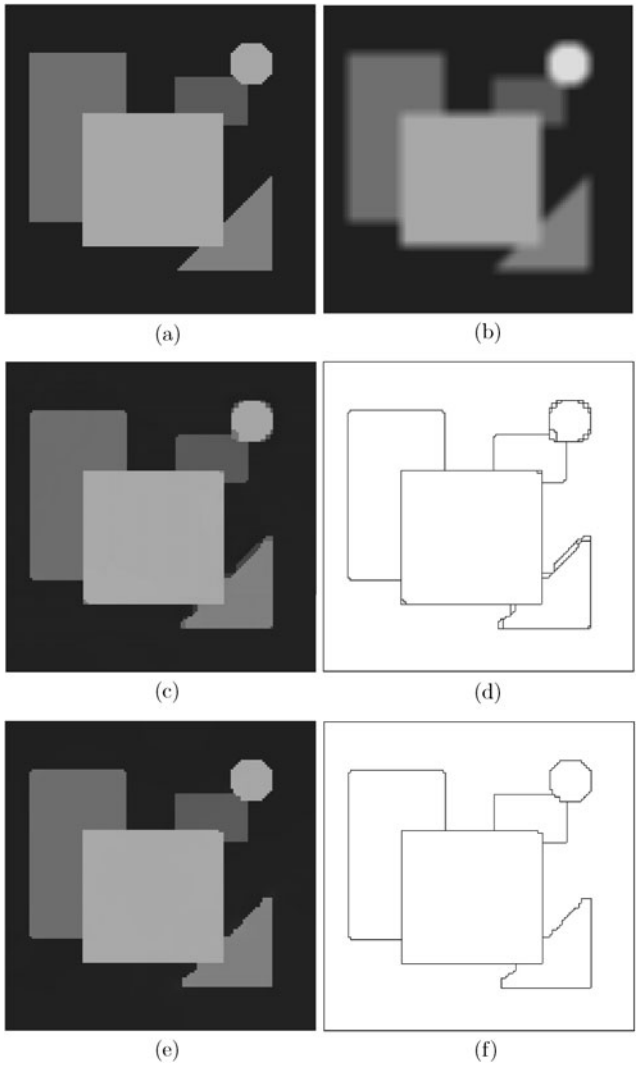

Fig. 6 (**a**) Image Synthetic2; (**b**) image Synthetic2 blurred by mask (19); (**c**) restoration obtained by Nikolova's algorithm ($\lambda = 1$ and $\alpha = 200$) and (**d**) its line elements; (**e**) restoration obtained by the CATILED algorithm with the non-parallelism constraint ($\lambda = 1$, $\alpha = 200$ and $\varepsilon = 1200$) and (**f**) its line elements

Fig. 5 Image in Fig. 4(b) restored by CATILED ($\lambda = 0.5$, $\alpha = 10$) after the minimization of the first approximation

Figures 4(c) and 4(e) exhibit the restorations of the image in Fig. 4(b) by Nikolova's algorithm and by the CATILED algorithm, respectively. The parameters used for these two algorithms are $\lambda = 0.5$ and $\alpha = 10$, and moreover $\varepsilon = 150$ in the CATILED algorithm. As we have seen in Sect. 7, the algorithm given by Nikolova in [23] is the subcase of CATILED when $\varepsilon = 0$.

Note that the role of $\varepsilon > 0$ in (9) is crucial in the CATILED algorithm, in order to get better restored images. Indeed, the line elements in Figs. 4(d) and 4(f) show how the CATILED algorithm inhibits parallel lines.

In Fig. 5 we present the reconstruction of the image in Fig. 4(b) obtained by the CATILED algorithm after the minimization of first convex approximation of the dual energy. The mean squared error with respect to original equal is to 14.7. This fact confirms what we have shown in Sect. 9, that is even the first approximation has already good properties of reconstruction.

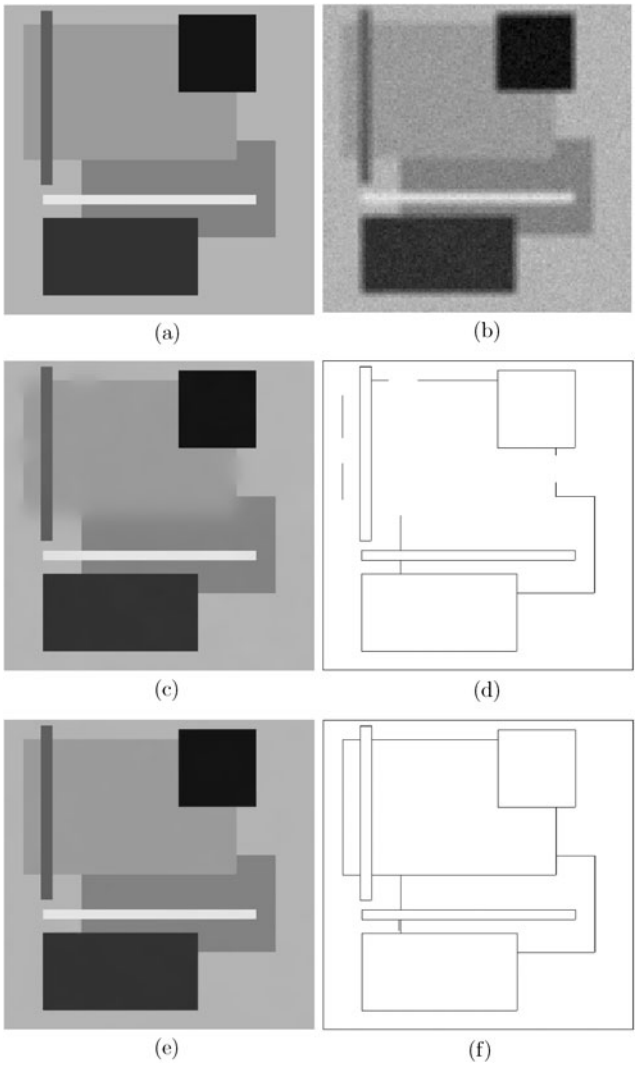

Fig. 7 (**a**) Image Synthetic3; (**b**) image Synthetic3 blurred by mask (19) and corrupted by noise ($\sigma^2 = 49$); (**c**) restoration obtained by Nikolova's algorithm ($\lambda = 4$ and $\alpha = 2000$) and (**d**) its line elements; (**e**) restoration obtained by the CATILED algorithm with the line continuation constraint ($\lambda = 4$, $\alpha = 2000$ and $\varepsilon = -900$) and (**f**) its line elements.

In Fig. 6(a) the next considered image, *Synthetic2*, of dimensions 128×128 appears. Figure 6(b) shows the image Synthetic2 blurred by the mask (19).

The restorations of the image in Fig. 6(b) by Nikolova's and by the CATILED algorithm are presented in Fig. 6(c) and 6(e), respectively. The parameters used for these two algorithms are $\lambda = 1$ and $\alpha = 200$, and moreover $\varepsilon = 1200$ for the CATILED algorithm. The line elements of the images in Figs. 6(c) and 6(e) are presented in Figs. 6(d) and 6(f).

Let us now consider the line continuation constraint. In Fig. 7(a) the 160×160 image *Synthetic3* appears. In Fig. 7(b) there is the image Synthetic3 blurred by the mask M_1 in (19) and corrupted by i.i.d. Gaussian noise of variance $\sigma^2 = 49$.

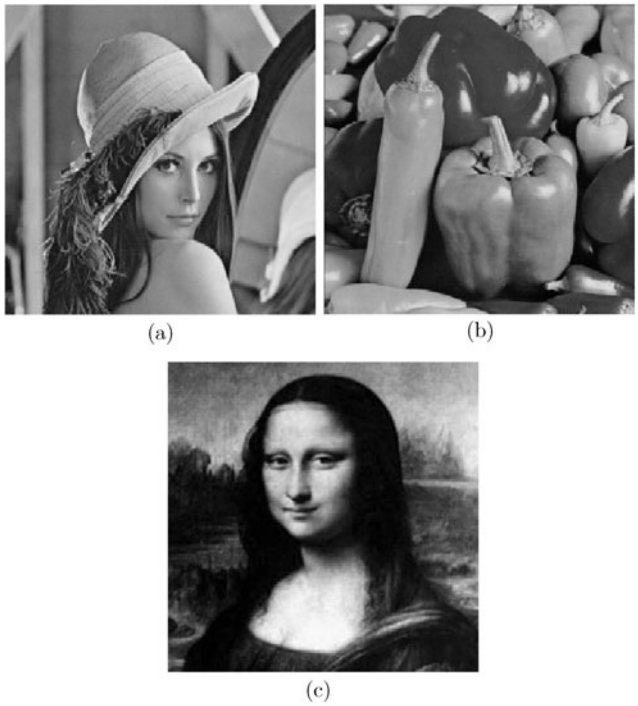

Fig. 8 (**a**) Image *Lena*; (**b**) Image *Peppers*; (**c**) Image *Monalisa*

Table 1 MSEs between images restored by difference operators of order $k = 1$ and either $\varepsilon = 0$ or $\varepsilon \neq 0$

image	$\varepsilon = 0$	$\varepsilon \neq 0$
Synthetic1	12.5	8.3
Synthetic2	11.2	7.9
Synthetic3	11.7	8.6

Figures 7(c) and 7(e) exhibit the restorations of the image in Fig. 7(b) by Nikolova's algorithm and by the CATILED algorithm, respectively. The parameters used for these two algorithms are $\lambda = 4$ and $\alpha = 2000$, and moreover $\varepsilon = -900$ in the CATILED algorithm.

In this case the role of $\varepsilon < 0$ in (9) is essential in the CATILED algorithm, in order to favor the line continuation as it is possible to see in Figs. 7(d) and 7(f).

In particular, the fact that ε could be taken not equal zero is essential in order to produce a low MSE (*Mean Squared Error*) between the reconstructed and the original images. The MSEs of the images for Figs. 4, 6 and 7 are given in Table 1 below.

Next we consider three different images of dimension 256×256: *Lena*, *Peppers* and *Monalisa* (see Fig. 8). These three images have been blurred using alternatively the blur

Table 2 MSEs between images restored by operators of order $k = 1, 2, 3$ and the original ones

image	blur	noise	$k = 1$	$k = 2$	$k = 3$
Lena	M_1	no	10.96	7.17	7.02
Lena	M_1	yes	11.94	9.96	10.05
Lena	M_2	no	10.46	6.56	6.36
Lena	M_2	yes	11.66	8.76	8.24
Peppers	M_1	no	9.55	5.35	5.47
Peppers	M_1	yes	11.21	8.71	8.52
Peppers	M_2	no	8.67	5.03	4.79
Peppers	M_2	yes	10.40	7.41	6.74
Monalisa	M_1	no	7.77	3.98	3.97
Monalisa	M_1	yes	9.53	6.47	6.07
Monalisa	M_2	no	6.97	2.92	2.78
Monalisa	M_2	yes	8.97	5.19	4.71

Fig. 9 (**a**) Image *Lena* blurred by mask M_1; (**b**) reconstruction using first order finite difference operators; (**c**) reconstruction using second order finite difference operators; (**d**) reconstruction using third order finite difference operators

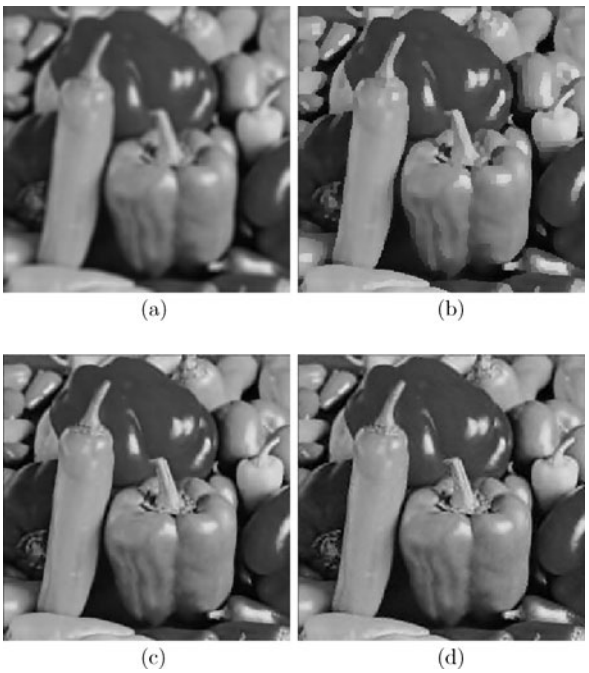

Fig. 10 (**a**) Image *Peppers* blurred by mask M_1; (**b**) reconstruction using first order finite difference operators; (**c**) reconstruction using second order finite difference operators; (**d**) reconstruction using third order finite difference operators

masks M_1 given in (19) and

$$M_2 = \begin{pmatrix} 0 & 5 & 10 & 5 & 0 \\ 5 & 25 & 50 & 25 & 5 \\ 10 & 50 & 50 & 50 & 10 \\ 5 & 25 & 50 & 25 & 5 \\ 0 & 5 & 10 & 5 & 0 \end{pmatrix}.$$

Moreover, we have also considered, as data, the blurred images corrupted by i.i.d. Gaussian noise with zero mean and variance $\sigma^2 = 25$. However, here we present the figures only of experimental results obtained with mask M_1 and without noise. Of course the final Table 2 *summarizes* all the results also in a quantitative objective manner.

In Fig. 9(a) there is *Lena* blurred by mask M_1. The restored image using first order finite difference operators, with $\lambda = 0.61$ and $\alpha = \varepsilon = 22.1$, is shown in Fig. 9(b). The image obtained by using second order operators with $\lambda = 0.43$ and $\alpha = \varepsilon = 0.72$ is given in Fig. 9(c). The third

order restoration using $\lambda = 0.34$ and $\alpha = \varepsilon = 0.88$ is presented in Fig. 9(d).

The blurred image of *Peppers* is presented in Fig. 10(a). The first order reconstruction is obtained by using $\lambda = 0.47$ and $\alpha = \varepsilon = 17.2$ and is shown in Fig. 10(b). The image obtained by using second order operators, with $\lambda = 0.33$ and $\alpha = \varepsilon = 0.51$, is given in Fig. 10(c), while the third order restoration, with $\lambda = 0.52$ and $\alpha = \varepsilon = 0.77$, is presented in Fig. 10(d).

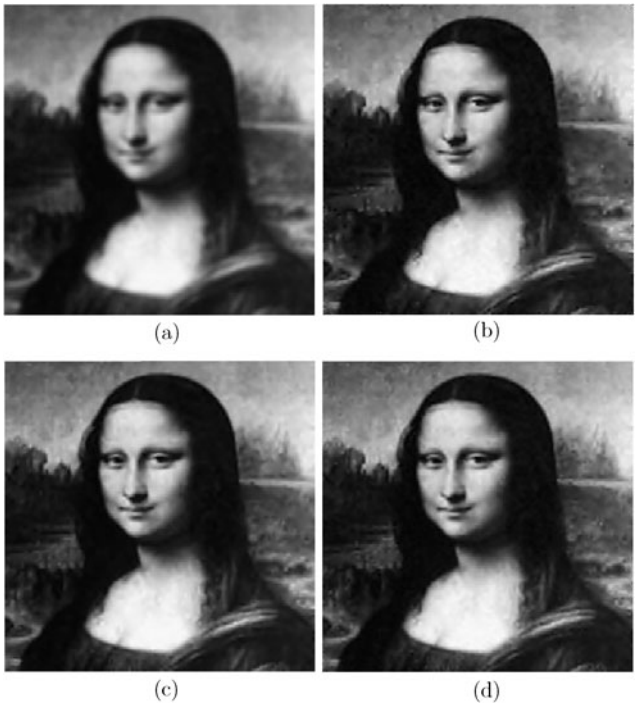

Fig. 11 (**a**) Image *Monalisa* blurred by mask M_1; (**b**) reconstruction using first order finite difference operators; (**c**) reconstruction using second order finite difference operators; (**d**) reconstruction using third order finite difference operators

In Fig. 11(a) appears *Monalisa* blurred by mask M_1. The first order reconstruction, with $\lambda = 0.61$ and $\alpha = \varepsilon = 12.6$, is shown in Fig. 11(b), the second order image reconstruction, with $\lambda = 0.43$ and $\alpha = \varepsilon = 0.67$, is given in Fig. 11(c), and the third order one, with $\lambda = 0.51$ and $\alpha = 0.73$, is presented in Fig. 11(d).

In Table 2 we report the MSE between the images restored by the CATILED algorithm, using alternatively finite difference operators of order $k = 1$, $k = 2$ and $k = 3$, and the original ones. Note that the MSEs obtained by CATILED with finite difference operators of order three in almost all these cases are the lowest.

The computational cost of the CATILED algorithm is proportional to the order of the finite difference operator used. Thus, sometimes the improvement of the quality obtained by using operators of order three, instead of those of order two, could not justify the increase of the computational cost. Indeed, the main difference appears from the case $k = 1$ and $k = 2$.

From the above argument and Table 2, we produce experimental results in the most interesting case $k = 2$, with $\varepsilon \in \{-\alpha, 0, \alpha\}$, considering alternately the non-parallelism and the continuation constraints. These results show how relevant is to take $\varepsilon \neq 0$ in order to minimize the MSEs. This phenomenon is illustrated in the next Table 3.

The final experiment is *real*, in the sense that we use a real photo taken during a sport action and not artificially blurred by us, see Figs. 12(a) and 12(c). The blur estimation is performed by the algorithm proposed in [17], while the parameter estimation is obtained by the technique introduced in [16]. The reconstructed images are given in Figs. 12(b) and 12(d), respectively.

Table 3 MSEs between the images restored using $\varepsilon \in \{-\alpha, 0, \alpha\}$ and the original ones

image	blur	noise	$\varepsilon = 0$	$\varepsilon = \alpha$	$\varepsilon = -\alpha$
Lena	M_1	no	9.27	7.17	7.01
Lena	M_1	yes	10.2	9.96	9.78
Lena	M_2	no	6.98	6.56	6.78
Lena	M_2	yes	10.56	8.76	8.88
Peppers	M_1	no	10.34	5.35	5.33
Peppers	M_1	yes	9.27	8.71	8.67
Peppers	M_2	no	7.11	5.03	4.91
Peppers	M_2	yes	8.22	7.41	6.98
Monalisa	M_1	no	5.21	3.98	4.12
Monalisa	M_1	yes	7.78	6.47	6.12
Monalisa	M_2	no	5.45	2.92	2.98
Monalisa	M_2	yes	8.11	5.19	5.21

Fig. 12 (**a**) Original image of *Bettega*; (**b**) reconstruction using the second order finite difference operator; (**c**) a detail of the original image of *Bettega*; (**d**) the same detail reconstructed using the second order finite difference operator

11 Conclusions

In this paper, we addressed the problem of restoring a blurred and noisy image. The solution is defined as a minimum of a suitable energy function. Such a function is the weighted sum of two terms: the former gives the faithfulness to data, the latter imposes regularity constraints on the solution. In particular we assumed that the ideal image is piecewise regular and must have thin or continuous edges. To minimize the energy function that implicitly refer to discontinuities, a new GNC type algorithm was proposed. The experimental results show how non-parallelism and the continuation constraints of the discontinuities are very important. Indeed, the images reconstructed by CATILED do not present double or discontinuous edges and this improves the quality of reconstructions. In particular, we showed that the first approximation of the dual energy, used in CATILED, is adequate, since it is possible to prove that it implicitly refers to discontinuities, by means of the duality Theorem 3. The technique does not use special matrix A, so that can be applied to several other related problems, as the reconstruction images in tomography. Even the blur is not required to be translation invariant. In Table 2 in Sect. 10 we reported the MSE between the original images and those restored, using alternatively differential operators of order $k = 1, 2, 3$. The main improvements arise from the cases $k = 2$ and $k = 3$.

Proof of Theorem 3

Let B and β satisfy (a) and (b) respectively. Using (5), we shall show that g verifies (c). Observe that it is possible to extend uniquely β to a continuous function $\overline{\beta} : \overline{B} \to \widetilde{\mathbb{R}} := \mathbb{R} \cup \{\infty\}$. We have:

$$g(t) = \inf_{b \in B} \{\lambda^2 b t^2 + \beta(b)\} = \min_{b \in \overline{B}} \{\lambda^2 b t^2 + \overline{\beta}(b)\} \tag{20}$$

for all $t \in \mathbb{R}$.

Clearly, g is even. To prove that $g \in \mathrm{Lip}_{\mathrm{loc}}(\mathbb{R})$, fix $0 \leq K_1 < K_2$, and choose $t_1, t_2 \in [K_1, K_2]$. From (20) there are $b_1, b_2 \in \overline{B}$ such that

$$\begin{aligned} g(t_1) &= \lambda^2 b_1 t_1^2 + \overline{\beta}(b_1), \\ g(t_2) &= \lambda^2 b_2 t_2^2 + \overline{\beta}(b_2), \end{aligned} \tag{21}$$

hence $\lambda^2 b_1 t_1^2 + \overline{\beta}(b_1) \leq \lambda^2 b_2 t_1^2 + \overline{\beta}(b_2)$, and $\lambda^2 b_2 t_2^2 + \overline{\beta}(b_2) \leq \lambda^2 b_1 t_2^2 + \overline{\beta}(b_1)$. Thus

$$\begin{aligned} g(t_1) - g(t_2) &\leq \lambda^2 b_2 t_1^2 + \overline{\beta}(b_2) - \lambda^2 b_2 t_2^2 - \overline{\beta}(b_2) \\ &= \lambda^2 b_2 \, (t_1 + t_2) \, (t_1 - t_2) \\ &\leq 2\lambda^2 \cdot \sup B \cdot K_2 \, |t_1 - t_2|; \end{aligned}$$

and similarly $g(t_2) - g(t_1) \leq 2\lambda^2 \cdot \sup B \cdot K_2 \, |t_1 - t_2|$. Consequently

$$|g(t_1) - g(t_2)| \leq 2\lambda^2 \cdot \sup B \cdot K_2 \, |t_1 - t_2|,$$

in other words $g \in \mathrm{Lip}_{\mathrm{loc}}(\mathbb{R})$.

To see that g is non-decreasing in $\mathbb{R}_0^+$, fix $t_1, t_2 \in \mathbb{R}_0^+$ with $t_1 > t_2 \geq 0$, and let b_1, b_2 be as in (21). Then

$$\begin{aligned} g(t_1) &= \lambda^2 b_1 t_1^2 + \overline{\beta}(b_1) \geq \lambda^2 b_1 t_2^2 + \overline{\beta}(b_1) \\ &\geq \lambda^2 b_2 t_2^2 + \overline{\beta}(b_2) = g(t_2), \end{aligned}$$

and the claim follows.

Let us show that $f(t) = g(\sqrt{t})$ satisfies (d) and (6). First of all, note that, by (b) and (20),

$$f(0) = \inf_{b \in B} \beta(b) = \lim_{b \to \sup B} \beta(b).$$

Hence (6) holds.

Clearly, since we have already shown that g satisfies (c), then it follows immediately that f is non-decreasing and continuous on $\mathbb{R}_0^+$.

We now prove that f is concave in $\mathbb{R}_0^+$. Given $t_0 \in \mathbb{R}_0^+$ and the line $r_0(t) = \lambda^2 b^* t + \overline{\beta}(b^*)$, where $b^* \in \overline{B}$ is an element of $\overline{B}$ attaining the minimum in (20) at $t = t_0$, that is

$$\begin{aligned} g(\sqrt{t_0}) = f(t_0) &= \min_{b \in \overline{B}} \{\lambda^2 b t_0 + \overline{\beta}(b)\} \\ &= \lambda^2 b^* t_0 + \overline{\beta}(b^*), \end{aligned}$$

we get $r_0(t) \geq f(t)$ in $\mathbb{R}_0^+$.

Note that f is the lower envelope of a family of lines, whose equations are given by

$$r(t) = \lambda^2 b\, t + \beta(b), \quad b \in B.$$

These lines are tangent to the graph of f at the points in which f is differentiable.

The function f is concave and continuous, and thus f' is non-increasing on its domain. The curve $y = f(x)$ admits the right tangent line at the point $(0, f(0))$. Indeed, by contradiction, if its angular coefficient were $\lambda^2 b = \infty$, then it should follow that B is not bounded, which contradicts assumption (a). Thus, f is differentiable at $t = 0$.

We shall show next that the set of points at which f is not differentiable is at most finite. To this aim, we observe that, if $b_1 > b_2 > b_3 \in B$ belong to the same interval I_j, and if (t_0, y_0) is the point of intersection of the lines

$$r_1(t) = \lambda^2 b_1\, t + \beta(b_1), \qquad r_3(t) = \lambda^2 b_3\, t + \beta(b_3)$$

and y_2 is the y-coordinate of the point of the line $r_2(t) = \lambda^2 b_2\, t + \beta(b_2)$ whose x-coordinate is t_0, then we have $y_2 < y_0$. Indeed, let $\tau \in (0, 1)$ be such that $b_2 = \tau\, b_1 + (1 - \tau)\, b_3$. By virtue of strict convexity of β in I_j, we get

$$\begin{aligned} y_2 - \lambda^2 b_2\, t_0 &= \beta(b_2) \\ &< \tau\, \beta(b_1) + (1-\tau)\beta(b_3) \\ &= \tau\, y_0 - \tau\, \lambda^2 b_1\, t_0 \\ &\quad + (1-\tau) y_0 - (1-\tau)\lambda^2 b_3 t_0 \\ &= y_0 - \lambda^2 b_2\, t_0, \end{aligned} \tag{22}$$

and thus $y_2 < y_0$. Let now $\bar{t} \in \mathbb{R}^+$ be a point of non-differentiability of f, and let us denote by $\lambda^2 b_s$ and $\lambda^2 b_d$ the values of left and right derivative of f in $\bar{t}$ respectively: we have $b_s > b_d$, by virtue of concavity of f. Let us now suppose that b_s and b_d belong to the same interval I_{j_0}, whose union forms the set $\overline{B}$. We note that in this case, since f is concave, then all lines having angular coefficient $\lambda^2 \widehat{b}$ between $\lambda^2 b_d$ and $\lambda^2 b_s$ are support lines for f in $(\bar{t}, f(\bar{t}))$. From (22) applied to $b_1 = b_s$, $b_2 = \widehat{b}$, $b_3 = b_d$, it follows that $(\bar{t}, f(\bar{t}))$ is not the intersection point of the lines

$$r_s(t) = \lambda^2 b_s\, t + \beta(b_s), \qquad r_d(t) = \lambda^2 b_d\, t + \beta(b_d).$$

Thus, every interval I_j contains at most two values of B corresponding to two different points of non-differentiability of f. From this and the fact that B is the union of a *finite* number of intervals or singletons it follows that f is differentiable up to the complement of a finite number of points.

Moreover, we note that every concave function, defined on an interval or halfline contained in $\mathbb{R}_0^+$, whose derivative f' exists in 0 and up to the complement of a finite set, has the property that f' is continuous on its domain. Indeed, in this case, this domain is the union of a halfline and eventually of open intervals; f' is non-increasing on each of these sets, and thus there either f' is continuous or f' admits points of discontinuity of the first kind: this last case is impossible, by virtue of the Darboux theorem. Thus f' is continuous on its domain.

Conversely, we prove that, if g and f satisfy (c) and (d) respectively, then there exist a set B and a function β for which (a) and (b) hold. Let Ξ be the set of all angular coefficients of the lines tangent to the graph of f at the points $(t_0, f(t_0))$ of differentiability of f. Let $B = \{\zeta/\lambda^2 : \zeta \in \Xi\}$. Since f is differentiable in 0 and f' is non-increasing and non-negative on its domain, then B is bounded and is contained in $\mathbb{R}_0^+$, with

$$f'(0) = \lambda^2 \cdot \sup B. \tag{23}$$

Moreover, since f' is defined in the union of a finite number of intervals or halflines, by applying the Darboux theorem to each of them we get that B is a finite union of intervals or singletons, which we denote by I_j, $j = 1, \ldots, m$. The sets I_j are nonoverlapping, since f' is non-increasing on its domain, namely $\overline{I_j} \cap \overline{I_l} = \emptyset \,\forall\, j \neq l$. Indeed, if there exists a point $t_0 \in \mathbb{R}^+$ at which f is not differentiable, then the left derivative of f at t_0 is strictly greater than its left derivative.

Given $b \in B$, define $\beta(b)$ as the intersection point between the y-axis and any line, tangent to the graph of f, whose angular coefficient is $\lambda^2 b$. The function β is well-defined: indeed, if we consider two tangent lines to the curve $y = f(x)$ at the points $(t_0, f(t_0))$ and $(t_1, f(t_1))$ with $t_0 < t_1$, then the intersection with the y-axis consists on a unique point, since, by virtue of concavity of f, the graph of this function between the points $(t_0, f(t_0))$ and $(t_1, f(t_1))$ is a segment.

Let $b_0, b_1 \in B$, with $b_0 < b_1$, and

$$r_0(t) = \lambda^2 b_0\, t + \beta(b_0), \qquad r_1(t) = \lambda^2 b_1\, t + \beta(b_1) \tag{24}$$

two lines, tangent to the curve $y = f(x)$ at the points $(t_0, f(t_0))$ and $(t_1, f(t_1))$ respectively. Hence $0 \leq t_1 < t_0$, since f is concave. The lines in (24) are not parallel, and, denoting by (t_2, y_2) their intersection point, we have:

$$r_0(t) > r_1(t) \quad \text{in } [0, t_2),$$

and so $\beta(b_0) = r_0(0) > r_1(0) = \beta(b_1)$; in other words β is strictly decreasing on B.

We now prove that β is strictly convex on each interval I_j. Let $b_1 > b_2 > b_3 \in I_j$, where

$$b_2 = \tau b_1 + (1 - \tau) b_3, \tag{25}$$

with $0 < \tau < 1$. Let (t_0, y_0), with $t_0 \in \mathbb{R}_0^+$, be the intersection point of the lines r_1, r_2 tangent to the graph of f, whose

angular coefficients are $\lambda^2 b_1$, $\lambda^2 b_2$ respectively. The line r_3 tangent to the graph of f, whose angular coefficient is $\lambda^2 b_3$, intersects r_1 and r_2 in the points (t_1, y_1) and (t_2, y_2) respectively. There are three cases: $t_0 < t_1 < t_2$, $t_2 < t_1 < t_0$, $t_1 = t_2 = t_0$. The last two cases cannot occur: otherwise the line r_2 would not belong to the lower envelope of f. Hence $t_0 < t_1 < t_2$ and so

$$\beta(b_1) = y_0 - \lambda^2 b_1 t_0, \qquad \beta(b_2) = y_0 - \lambda^2 b_2 t_0,$$

$$\beta(b_3) > y_0 - \lambda^2 b_3 t_0.$$

From this and (25) it follows that

$$\begin{aligned}\beta(b_2) &= \tau y_0 + (1-\tau) y_0 - \tau\lambda^2 b_1 t_0 - (1-\tau)\lambda^2 b_3 t_0 \\ &< \tau\,\beta(b_1) + (1-\tau)\beta(b_3).\end{aligned}$$

This proves that β is strictly convex on each I_j.

Note that β is continuous at the interior points of each I_j, since β is strictly convex in I_j. Let us show that β is continuous at the left endpoints, say for simplicity b_0, of these intervals I_j, with $b_0 \in I_j$. To each b_0 put

$$T_0 = \{t \in \mathbb{R}_0^+ : f'(t) = \lambda^2 b_0\}.$$

By construction of B, we get that $T_0 \neq \emptyset$.

Let $t_0 = \inf T_0$, and consider first the case $t_0 = 0$. Then, clearly $0 = \min T_0$; and from this it follows that

$$\lambda^2 b_0 = f'(0) = \lambda^2 \cdot \sup B,$$

by (23). Thus, by definition of b_0, we get that $j = m$ and $I_m = \{b_0\}$, and thus β is continuous at b_0.

We now consider the case $t_0 > 0$: first of all, we note that t_0 belongs to the topological closure of T_0.

Let us prove that $t_0 \notin T_0$: otherwise $t_0 = \min T_0$ and t_0 is a point of differentiability of f. From this and from the hypotheses it follows that there exists a neighborhood V of t_0, such that f' is continuous and strictly decreasing on V: thus the function f'/λ^2 attains all values belonging to a suitable neighborhood containing b_0. This is impossible, since b_0 does not belong to the interior of I_j. Thus t_0 is a limit point for T_0, and from monotonicity of f' it follows that T_0 contains a right neighborhood of t_0, with the exception of the point t_0. By virtue of the L'Hospital theorem we get that $f'_d(t_0) = \lambda^2 b_0$. If t_0 is a point of non-differentiability of f, then $f'_s(t_0) > f'_d(t_0)$, and thus there exists $b_1 > b_0$ such that $(b_0, b_1) \subset \mathbb{R} \setminus B$. From this it follows that $I_j = \{b_0\}$, and hence β is continuous at b_0. Let now t_0 be a differentiability point of f: if there exists $t^* \in (0, t_0)$ such that $f'(t^*) = \lambda^2 b_0$, then t_0 is not the infimum of the set T_0, which is impossible. From this and assumption (d) it follows that there exists a left neighborhood U of t_0, such that f' is continuous and strictly decreasing on U. Thus f' has the inverse function ω, defined in a suitable interval V, whose left endpoint is b_0, and continuous on V. We have:

$$\beta(b) = f(\omega(b)) - \lambda^2 b\,\omega(b), \quad \forall\, b \in V.$$

From this it follows that β is continuous at b_0.

We now prove that β is continuous at the right endpoints, which in general we denote by b_1, of the intervals I_j, with $b_1 \in I_j$. If β is not continuous in b_1, then from strict convexity it follows

$$\lim_{x \to b_1^-} \frac{\beta(b_1) - \beta(x)}{b_1 - x} = \infty,$$

and hence $\beta(b_1) > \beta(x)$ for each x belonging to a suitable left neighborhood of b_1, that is β is not strictly decreasing. This is impossible by what was proved above.

We next prove that β is bounded from below. Since f' attains its maximum at $t = 0$, the formula (23) holds, and since the intersection between the tangent line at 0 and the y-axis is $f(0)$, then

$$\inf_{b \in B} \beta(b) = \lim_{b \to \sup B} \beta(b) = \lim_{b \to f'(0)/\lambda^2} \beta(b) = f(0).$$

Thus β is bounded from below by $f(0)$, and (6) holds.

Finally we prove that β satisfies (5). For every $b \in B$, the line $r_0(t) = \lambda^2 b\, t + \beta(b)$ is tangent to the curve $y = f(x)$ at the point $(t_0, f(t_0))$, and $b = f'(t_0)/\lambda^2$. Since f is concave, we have, $\forall\, t \in \mathbb{R}_0^+$, $\forall\, b \in B$:

$$f(t) \leq \lambda^2 b\, t + \beta(b).$$

Taking the infimum with respect to $b \in B$, we get:

$$f(t) \leq \inf_{b \in B} \{\lambda^2 b\, t + \beta(b)\} \quad \forall\, t \in \mathbb{R}_0^+. \tag{26}$$

Moreover, from the definition of β and of tangent line, we get

$$\begin{aligned}\inf_{b \in B} \{\lambda^2 b\, t + \beta(b)\} &\leq f'(t)\, t + \beta\left(\frac{f'(t)}{\lambda^2}\right) \\ &= f(t),\end{aligned} \tag{27}$$

and thus, from (26) and (27), we obtain

$$f(t) = \inf_{b \in B} \{\lambda^2 b\, t + \beta(b)\},$$

that is β satisfies condition (5). This completes the proof of Theorem 3.

Acknowledgement The second author has been partly supported by the MIUR-PRIN 2008 Project *Problemi di algebra lineare numerica strutturata: analisi, algoritmi, e applicazioni*, N. 20083KLJEZ, while the third author by the MIUR-PRIN 2009 Project *Metodi Variazionali ed Equazioni Differenziali alle Derivate Parziali Non Lineari*.

References

1. Aubert, G., Kornprobst, P.: Mathematical Problems in Image Processing. Springer, New York (2002)
2. Bedini, L., Gerace, I.: A deterministic algorithm for reconstruction images with interacting discontinuities. CVGIP, Graph. Models Image Process. **56**, 109–123 (1994)
3. Bedini, L., Tonazzini, A.: Fast fully data-driven image restoration by means of edge-preserving regularization. Real-Time Imaging **7**, 3–19 (2001)
4. Bedini, L., Gerace, I., Tonazzini, A.: A GNC algorithm for constrained images reconstruction with continuous-valued line processes. Pattern Recognit. Lett. **15**, 907–918 (1994)
5. Bedini, L., Gerace, I., Salerno, E., Tonazzini, A.: Models and algorithms for edge-preserving image reconstruction. Adv. Imaging Electron Phys. **97**, 86–189 (1996)
6. Bertero, M., Boccacci, P.: Introduction to Inverse Problems in Imaging Institute. Philadelphia, Bristol (1998)
7. Blake, A.: Comparison of the efficiency of deterministic and stochastic algorithms for visual reconstruction. IEEE Trans. Pattern Anal. Mach. Intell. **11**, 2–12 (1989)
8. Blake, A., Zisserman, A.: Visual Reconstruction. MIT Press, Cambridge (1987)
9. Bouman, C., Sauer, K.: A generalized Gaussian image model for edge-preserving MAP estimation. IEEE Trans. Image Process. **2**, 296–310 (1993)
10. Brewster, M.E., Kannan, R.: Nonlinear successive over-relaxation. Numer. Math. **44**, 309–315 (1984)
11. Charbonnier, P., Blanc-Féraud, L., Aubert, G., Barlaud, M.: Deterministic edge-preserving regularization in computed imaging. IEEE Trans. Image Process. **6**, 298–311 (1997)
12. Demoment, G.: Image reconstruction and restoration: overview of common estimation structures and problems. IEEE Trans. Acoust. Speech Signal Process. **37**, 2024–2036 (1989)
13. Fedeli, L., Gerace, I., Martinelli, F.: Unsupervised blind separation and deblurring of mixtures of sources. In: LNAI, vol. 4694, pp. 25–32 (2007)
14. Geman, S., Geman, D.: Stochastic relaxation, Gibbs distributions, and the Bayesian restoration of images. IEEE Trans. Pattern Anal. Mach. Intell. **6**, 721–740 (1984)
15. Geman, D., Reynolds, G.: Constrained restoration and the recovery of discontinuities. IEEE Trans. Pattern Anal. Mach. Intell. **14**, 367–383 (1992)
16. Gerace, I., Martinelli, F.: On regularization parameters estimation in edge-preserving image reconstruction. In: LNCS, vol. 5073, pp. 1170–1183 (2008)
17. Gerace, I., Pandolfi, R., Pucci, P.: A new estimation of blur in the blind restoration problems. In: Proc. ICIP'03, p. 4 (2003)
18. Gerace, I., Mastroleo, M., Milani, A., Moraglia, S.: Genetic blind image restoration with dynamical local evaluation. In: Proceeding of ICCSA, pp. 497–506. IEEE Comput. Soc., Los Alamitos (2008)
19. Gerace, I., Pinca, L., Pucci, P., Sanchini, G.: Surface image reconstruction for the comet assay technique. Int. J. Signal Imaging Syst. Eng. **1**, 10 (2008)
20. Hansen, P.C.: Analysis of discrete Ill-posed problems by means of the L-curve. SIAM Rev. **34**, 561–580 (1992)
21. Hansen, P.C., O'Leary, D.P.: The use of the L-curve in the regularization of discrete Ill-posed problems. SIAM J. Sci. Comput. **14**, 1487–1503 (1993)
22. Li, S.Z.: Roof-edge preserving image smoothing based on MRFs. IEEE Trans. Image Process. **9**, 1134–1138 (2000)
23. Nikolova, M.: Markovian reconstruction using a GNC approach. IEEE Trans. Image Process. **8**, 1204–1220 (1999)
24. Nikolova, M.: Thresholding implied by truncated quadratic regularization. IEEE Trans. Signal Process. **48**, 3437–3450 (2000)
25. Nikolova, M., Ng, M.K., Zhang, S., Ching, W.-K.: Efficient reconstruction of piecewise constant images using nonsmooth nonconvex minimization. SIAM J. Imaging Sci. **1**, 2–25 (2008)
26. Tonazzini, A., Bedini, L.: Degradation identification and model parameter estimation in discontinuity-adaptive visual reconstruction. Adv. Imaging Electron Phys. **120**, 193–284 (2002)

Antonio Boccuto was born in Catanzaro, Italy, on November 4, 1964. He received the degree in Mathematics from the University of Perugia, Italy, in 1987 and the Ph.D. degree in Mathematical Analysis from the Mathematical Institute of the Slovak Academy of Sciences in Bratislava, Slovakia, in 2000. He received the habilitation in Mathematics to Associate Professor from the Comenius University in Bratislava in 2008. He has been a researcher in Mathematical Analysis at University of Perugia since the Academic Year 1991/1992. His research interests include Real Analysis, Measure Theory and Integration, Nonlinear Partial Differential Equations, Approximation Theory.

Ivan Gerace was born in Cosenza, Italy, on December 10, 1967. He received the degree in Computer Science from the University of Pisa, Italy, in 1992, and the Ph.D. degree in Computational Mathematics and Operational Research from the University of Milan, Italy, in 1999. He has been an Assistant Professor of Numerical Analysis since May 2000 at the University of Perugia, Italy. His research interests include Image Processing, Numerical Linear Algebra, and Computational Complexity.

Patrizia Pucci was born in Perugia, Italy, on May 11, 1952. She received the degree in Mathematics from the University of Perugia in 1975. She has been full professor in Mathematical Analysis since the Academic Year 1987/1988 and is currently full professor at the University of Perugia. She received the 2004 Prize Prof. Luigi Tartufari for Mathematics, awarded by the Accademia Nazionale dei Lincei, Rome, Italy. Her research interests include Nonlinear Partial Differential Equations, Critical Point Theory, Variational Methods.